
ANALYSIS: GENERATIVE ADVERSARIAL NETWORKS FOR PCG ARRHYTHMIA DETECTION

SR-TEEM2-013

February 28, 2021

Contents

1 PCG-Net: GAN Visualization	2
1.1 Dense Generator Noise	2
1.2 Convolutional Discriminator Class Activation Maps	2
2 Results	2
2.1 PCG-Net: Testing Sample Distributions	2
2.2 PCG-Net: Generalization Statistics	3
2.3 PCG-Net: Dataset Feature Visualization	5
2.4 PCG-Net: Confusion Matrix	5
2.5 PCG-Net: Time Complexity	6
2.6 PCG-Net: Statistical Significance	6
2.7 VQGAN: PCG Construction Visualization	6
2.8 VQGAN: Testing Sample Distributions	7
2.9 Real-World Test	8
2.10 Classification Application	9
3 Discussion	9
4 Further Exploration and Application	9
5 Acknowledgement	9
6 Code Availability	9
7 Raw Data	9
7.1 PCG-Net	9
7.2 VQGAN	12
8 References	15

1 PCG-Net: GAN Visualization

1.1 Dense Generator Noise



Figure 8: Plot of the noise (artifact class) generated from the generator.

Figure 8 shows the input values (seeds) and corresponding generated noise. The variance in amplitudes and periods in the signal mimics that of real heartbeats changing. At a closer examination of the results, the generator appears to resample the seed values to that of the output (2500). This is expected as the generator consists of dense layers, which linearly increase the signal length and complexity

1.2 Convolutional Discriminator Class Activation Maps

Figure 10 visualizes the channels of the convolutional layers, which are responsible for extracting features from an inputted signal. The color of the vertical line represents the importance of the feature relative to other features. Meaning, the lighter the color, the more important the feature. As the input travels deeper into the model, the extractions get more complex. This is clearly shown by the distinct increase in coloration between layers one and two. This indicates that the layers are extracting latent features from the signal. The first convolutional plot depicts the extraction of important biomarkers, such as S1 and S2. In the next two layers, the extractions make it clear that the S1 sound is more important, as those are the brightest throughout all layers. This parallels medical knowledge, as most cardiovascular anomalies occur in Systole, or at the start of S1.

2 Results

2.1 PCG-Net: Testing Sample Distributions

Figure 13 illustrate that the GAN's accuracy, specificity, and sensitivity are skewed to the left. This suggests that the model is extremely successful at differentiating between abnormal and normal heart sounds.

The specificity distribution has a mean of 0.9030, with a standard deviation of 0.0547. The best model reached a specificity of 0.9672. This suggests that 90.3% of normal heart sounds were correctly identified.

The sensitivity distribution has a mean of 0.9952, with a standard deviation of 0.0197. The best model reached a sensitivity of 1.0. This suggests that 99.5% of abnormal heart sounds were correctly identified. In detecting pathologies in medicine, we often attempt to maximize sensitivity, the rate at which a subject with a disease is correctly identified amongst other ill subjects. This is because we want to ensure that all potential subjects with a disease are sent for further examination. Essentially, weighting sensitivity higher than specificity, the rate of correctly identified normal or healthy patients from a sample of healthy patients. Thus, from the results, the proposed model is robust, in that it can detect abnormalities nearly 100% of the time.

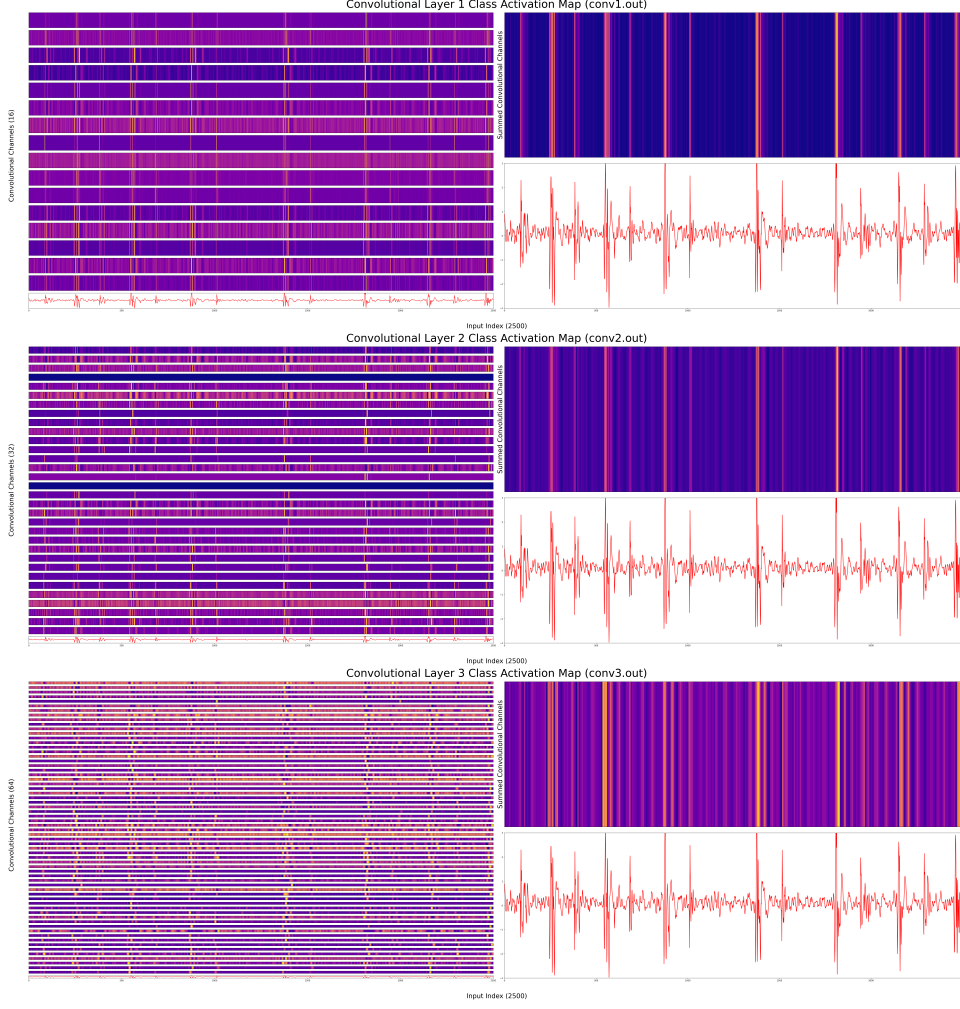


Figure 10: Normal activation maps of convolutional layers of the PCG-Net discriminator.

The accuracy distribution has a mean of 0.9498, with a standard deviation of 0.0293. The best model reached an accuracy of 0.9875. This suggests that 95.0% of both abnormal and normal sounds were classified correctly.

2.2 PCG-Net: Generalization Statistics

Generalization is important in creating accurate predictions, as it establishes that the model is learning meaningful features that are not just applicable to the training data, but signals overall. Figure 14 plots the loss and accuracy of the training and validation set over each epoch. The large fluctuations in the training set metrics are caused by logging the metrics after each step in the training set (on every change in the model parameters). Thus, the optimizer is bound to decrease gradients in the wrong direction, thus correcting for such variations cause those fluctuations. Both lines on the loss plot resemble an exponential curve, which suggests the model continues to learn as training progresses. The average deviation between the validation and training set for each epoch is 0.4817; though this deviation is high, it is due to the lack of meaningful surface-level features that would lead to accurate detection. Meaning, the model's deep feature extraction layers are responsible for the gap. Furthermore, the accuracy plots follow a logarithmic curve. In other words, as the training accuracy increasing, the validation correspondingly increases, though at a slower rate. Both graphs illustrate the model has reached convergence by the end of the training phase. This is confirmed by the static change in metrics in both datasets.

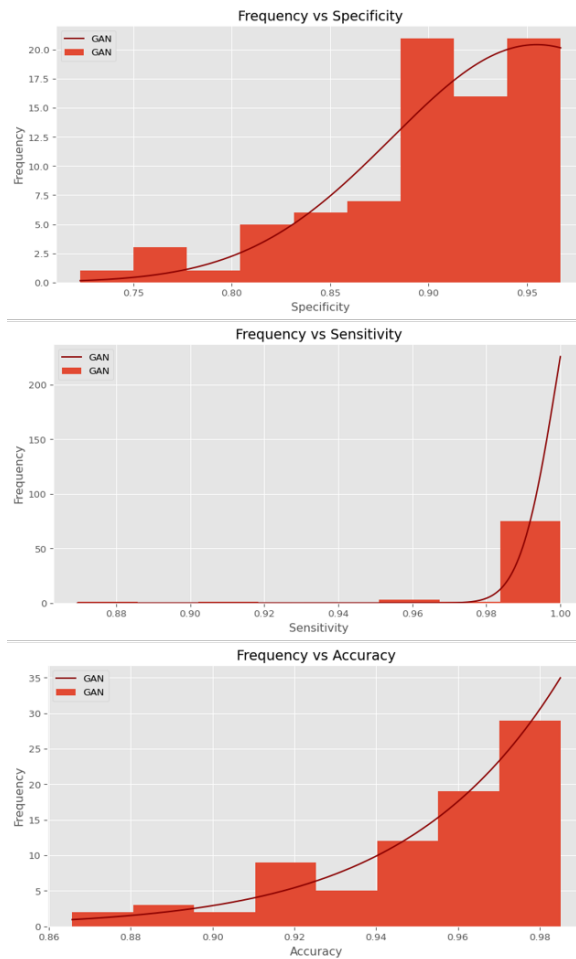


Figure 13: Plot of testing set results on specificity, sensitivity, and accuracy

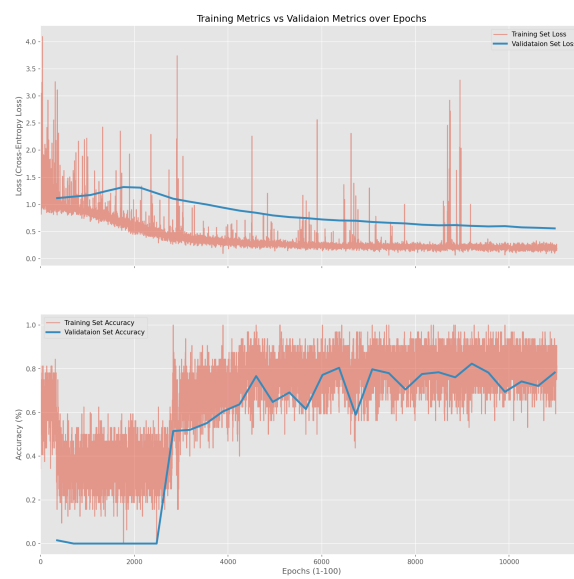


Figure 14: Plot of validation and training set accuracy and loss over 100 epochs.

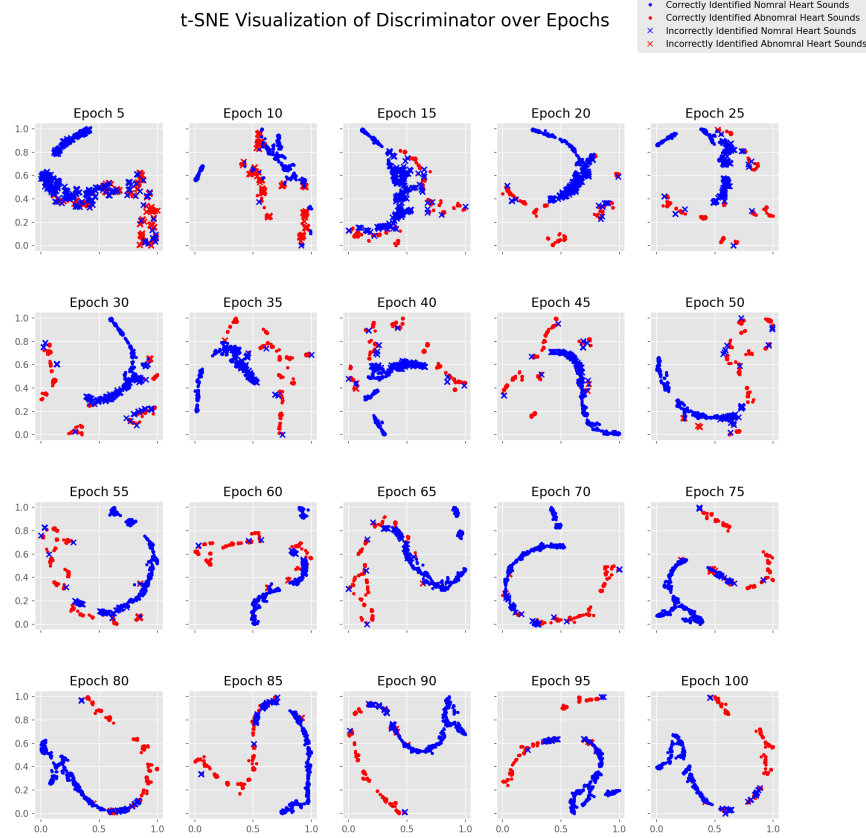


Figure 15: Plot of t-SNE visualizations over 100 epochs of the validation set.

2.3 PCG-Net: Dataset Feature Visualization

Dataset visualization is critical in understanding the dataset's complexity and model's effectiveness. Here, we use t-distributed stochastic neighbor embedding (t-SNE), a statistical method for visualizing multi-dimensional data in less computationally expensive dimensions. The method is presented with the raw prediction values for each input of the validation set and maps the corresponding predictions into a 2-dimensional space. Tracked over epochs, the visualization allows us to view the progression of the model's competence while training. The visualization highlights clear clustering within the dataset, which suggests the model is stable. Though, from epochs 70 and onwards, it is evident that there is overlapping between abnormal and normal signals. Assuming these signals as ground truth, this implies that additional feature engineering is required to adequately classify heart sounds.

2.4 PCG-Net: Confusion Matrix

The confusion matrix (Figure 16) aids in illustrating the performance for each class of the proposed method. Specifically, we evaluated the model's success on the grounds of average accuracy, specificity, and sensitivity of the classification. We calculated the average true positives, false positives, etc. for all 150 trials of the testing set. Using these floored values, we normalized each label along the y-axis. The matrix reveals that the most common misunderstanding occurs in predicting a normal heart sound, this is not surprising as the model is trained to be biased in detecting abnormal heart sounds. However, this occurs at the cost of specificity, which decreases the average normal misclassification rate to 8.1%. Overall, we conclude that the average accuracy of abnormal heartbeat detection is 95% with a misclassification rate of just 5%. Thus, the model is extremely accurate in detecting abnormalities in heart sounds and has the capabilities to further classify abnormal heart sounds into labeled arrhythmias.

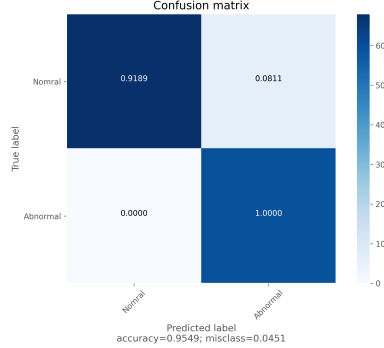


Figure 16: Matrix of accuracy between labels in the dataset.

2.5 PCG-Net: Time Complexity

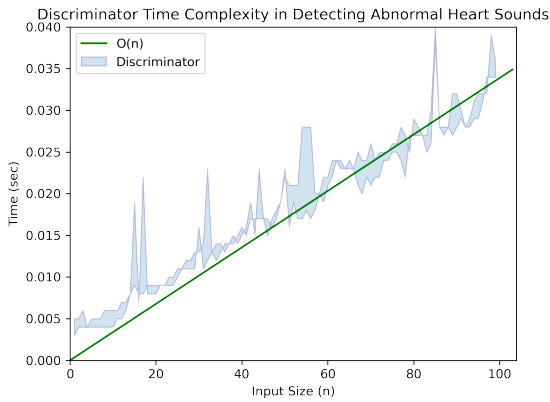


Figure 17: Time complexity of discriminator in classifying heart sounds.

Model complexity is used to gauge and evaluate the efficacy of a model against an increase in data (n). We mainly focus on time complexity as it is most relevant to the problem at hand (space complexity is $O(1)$). Depending on model deployment and integration, the complexity can vary. For example, GPUs have parallel processing capabilities, which allow them to process multiple signals at once, efficiently decreasing the model complexity to $O(1)$. For this reason, we use the worst-case scenario (a CPU), for analysis of the proposed method's time complexity. Figure 17 implies the model's time complexity is directly and linearly correlated to the input size, suggesting the complexity is $O(n)$. Thus, the model on average, can predict 2800 heart sounds in the worst case scenario. This will prove to be greatly helpful in real-time detection.

2.6 PCG-Net: Statistical Significance

From the p-values shown, we can conclude that all metrics were statistically significant because all p-values were less than 0.05. This implies that the null hypothesis can be rejected and the alternative hypothesis is accepted. The decrease in specificity is expected because we prioritized sensitivity over specificity to maximize the true positive rate, the percent of correctly identified abnormal heart sounds from a sample of only abnormal heart sounds.

2.7 VQGAN: PCG Construction Visualization

Figure 21 show the progression of heart sound construction from ECGs over epochs of the validation set. Ideally, he would want the reconstruction of the PCG spectrogram to identical to that of the ground truth. In practice, this doesn't occur, some features may be lost in the latent representation of the ECG spectrogram. These missing features will cause a spatial anti-aliasing effect, as the latent space doesn't have the dimensionality to extract pixel-to-pixel information. The series of spectrograms show the development of features in the latent space through the epochs. For example, the

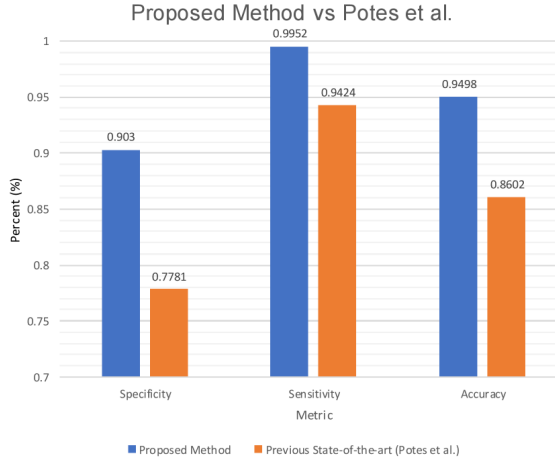


Figure 18: Comparison previous state-of-the-art and proposed method in specificity, sensitivity, and accuracy

Specificity	Sensitivity	Accuracy
1.65E-10	1.54E-77	1.07E-11

Figure 19: P-values from Proposed Method vs Potes et al.

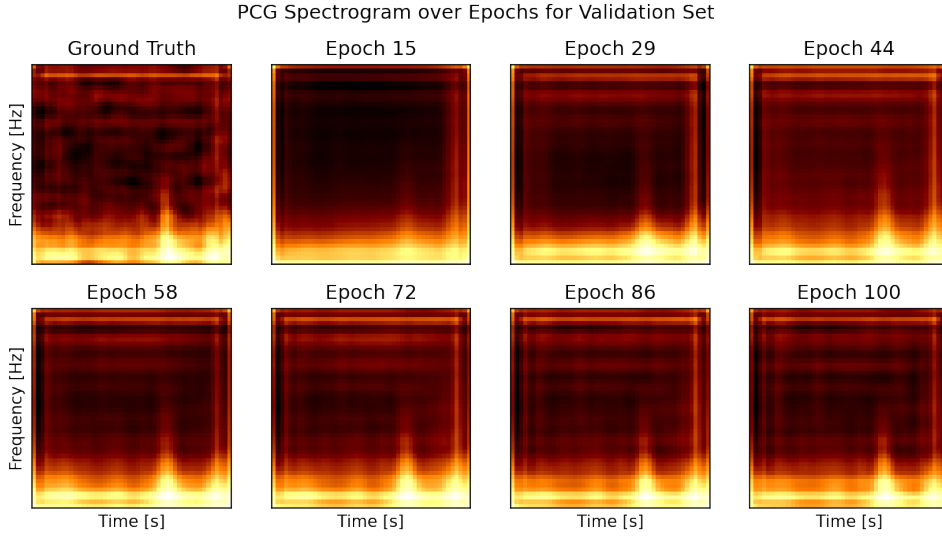


Figure 21: Plot of PCG spectrograms over epochs

frequency of the first peak (S1) varies significantly until the 86th epoch. This feature is important because it determines the rate of the S1 or "lub" sound; thus, creating the illusion that the sound is occurring faster relative to the ground truth. Furthermore, the S2 marker is severely softened, this is due to the rapid change in frequencies surrounding the marker and the light vertical bars to the right in each spectrogram. This suggests that much of the information regarding S2 will be lost when converting the spectrogram into a wave signal.

2.8 VQGAN: Testing Sample Distributions

Figure 23 shows that the VQGAN's loss is skewed to the right, but still has a large amount of variability. This suggests that the model has the ability to construct PCG spectrograms, but has a difficult time accurately constructing all spectrograms. This is supported by both the mean loss - 1.34, and the standard deviation - 0.258, as both values convey a high level of variance. We believe the inconsistencies are caused by the narrow gap of meaning full data. Markers,

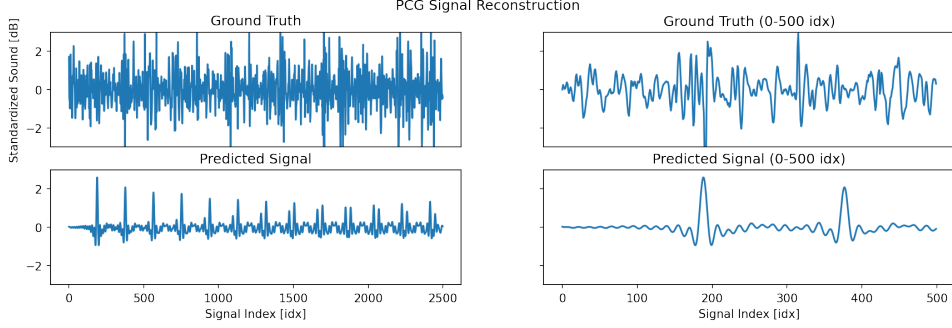


Figure 22: PCG construction accuracy.

such as S1 and S2, only occur for a narrow amount of time relative to the signal size. Thus, the majority of the signal's data is nonimportant and contains background noise.

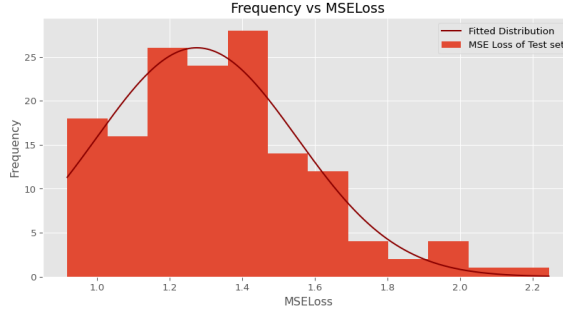


Figure 23: Distribution plot of testing results from PCG spectrogram construction.

2.9 Real-World Test

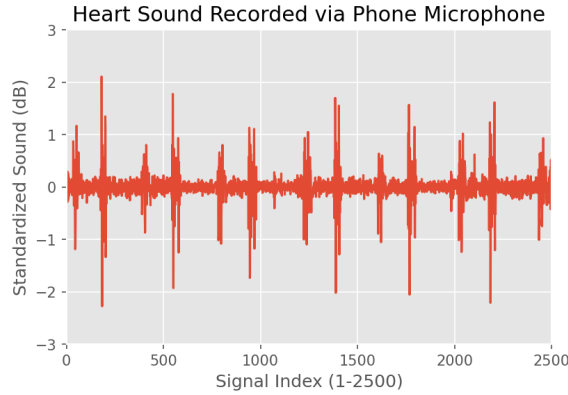


Figure 24: Plot of heart sound recording taken from a phone microphone.

Testing the model's viability is crucial for ensuring the model's success in the real world. Ideally, recording heart sounds are recorded with digital stethoscopes. These tools use transducer technology to convert sound into an electrical signal. Over the past decade, this technology has grown immensely (by cause of speech recognition). Modern phones have the potential to record the sounds at a high resolution, given the microphone is located at the correct position relative to the heart. Such a device will prove to extremely beneficial in providing diagnosis without the need for specialized equipment. 24 shows a heart sound recording from a phone microphone. The plot shows that important biomarkers, like S1 and S2, remain visible. This ensures that the recording doesn't contain excessive amounts of noise that may hinder the performance of the detection system. Hence, feeding it into the proposed method resulted in a normal classification.

2.10 Classification Application

3 Discussion

We proposed a Generative Adversarial Network (GAN), composed of a Dense Generator and a Convolutional Neural Network (CNN) Discriminator to detect abnormal heart sounds in a recording. The model achieved an accuracy of 94.98%, a specificity of 90.30%, and a sensitivity of 99.52% on the testing set. The previous state-of-the-art achieved an accuracy of 86.02%, a specificity of 77.81%, and a sensitivity of 94.24%. This data, along with results from the t-test revealed that the proposed alternative hypothesis was correct and that the null hypothesis should be rejected. This is because the proposed method reached better performance than the previous state-of-the-art methods. Additionally, the model attained a staggering 2500 classification per second in the worst-case scenario. This is because of the nature of the CNN architecture; unlike other methods, the CNN's reduce the data dimensionality as it forward propagates through the model. Furthermore, the proposed method showed real-world deployment capabilities for autonomous heart sound abnormality detection with recordings collected from a phone microphone. This test shows extremely promising results for future applications and integrations.

We also set out to introduce new pathologies for increased arrhythmia labels in classification. We proposed using a VQGAN for constructing PCG signals from existing ECG datasets that contain a surplus amount of arrhythmia-specific data. The results were promising, in that the VQGAN discriminator was able to construct the general shape of the PCG spectrogram, but missed import details in the fluctuation of important biomarkers (S1 and S2). This caused the PCG waveform representation extracted from the PCG spectrogram to miss rapid oscillations present in the biomarkers.

The object of this study was to create a fast and accurate end-to-end heart sound arrhythmia detection system, capable of detecting abnormalities in real-time without specialized equipment. While also increasing the number of cardiovascular pathologies classified. With the data shown, our proposed method accomplishes exemplary statistics in abnormalities detection and shows promising results in increased arrhythmia construction. Hopefully, this study will shed light on PCG construction techniques and give birth to applications with autonomous abnormality detection.

4 Further Exploration and Application

1. Deploying the model with an app that is available to 3rd world countries that can't afford to conduct in-depth testing regularly
 - (a) Integrate and serve the model using FastAPI
2. Use abnormal heart sound unsupervised datasets as a basis of categorical arrhythmia classification
 - (a) Using low dimensional visualization techniques like t-SNE or UMAP
 - (b) Cluster data using methods like K means and hierarchical clustering
3. Create a classifiable latent representation of PCG signal biomarkers that can be represented with accuracy and precision
 - (a) Created by VAE that are fed the PCG signals directly instead of a spectrogram
4. Investigate training a heart sound discriminator from generated PCG data from ECG datasets
5. Reconstructing speech (wav) recordings from the human auditory cortex (EEG) using techniques used for PCG construction

5 Acknowledgement

I thank Professor Lifang He of Leigh University for helpful feedback on the experiments and references.

6 Code Availability

All code used in this project is available at <https://git.io/JtAuU> and <https://git.io/JtAuO>. All models were run on Google's Colab service with PyTorch and PyTorch Lightning as the framework.

7 Raw Data

7.1 PCG-Net

Table 1: The table shows the accuracy, sensitivity, and specificity of 150 trials of training the GAN model on the dataset. The metrics displayed are the results of the testing set.

Trials	Specificity	Sensitivity	Accuracy
Trials 1	0.9375	0.971429	0.955224
Trials 2	0.955224	1	0.977612
Trials 3	0.898551	1	0.947761
Trials 4	0.935484	1	0.970149
Trials 5	0.967213	1	0.985075
Trials 6	0.90625	1	0.955224
Trials 7	0.955224	1	0.977612
Trials 8	0.855072	1	0.925373
Trials 9	0.935484	1	0.970149
Trials 10	0.967213	1	0.985075
Trials 11	0.90625	1	0.955224
Trials 12	0.955224	1	0.977612
Trials 13	0.811594	1	0.902985
Trials 14	0.935484	1	0.970149
Trials 15	0.967213	1	0.985075
Trials 16	0.90625	1	0.955224
Trials 17	0.955224	1	0.977612
Trials 18	0.884058	1	0.940299
Trials 19	0.935484	1	0.970149
Trials 20	0.967213	1	0.985075
Trials 21	0.921875	1	0.962687
Trials 22	0.955224	1	0.977612
Trials 23	0.855072	1	0.925373
Trials 24	0.935484	1	0.970149
Trials 25	0.967213	1	0.985075
Trials 26	0.90625	1	0.955224
Trials 27	0.955224	1	0.977612
Trials 28	0.768116	1	0.880597
Trials 29	0.935484	1	0.970149
Trials 30	0.967213	1	0.985075
Trials 31	0.90625	1	0.955224
Trials 32	0.790323	1	0.902985
Trials 33	0.806452	1	0.910448
Trials 34	0.847458	1	0.932836
Trials 35	0.955224	1	0.977612
Trials 36	0.847458	1	0.932836
Trials 37	0.917808	1	0.921224
Trials 38	0.885246	1	0.947761
Trials 39	0.915493	1	0.955224
Trials 40	0.768116	1	0.880597
Trials 41	0.915493	1	0.955224
Trials 42	0.944444	1	0.970149
Trials 43	0.90625	1	0.955224
Trials 44	0.891892	1	0.940299
Trials 45	0.851351	1	0.91791
Trials 46	0.955224	1	0.977612
Trials 47	0.955224	1	0.977612
Trials 48	0.876923	0.869565	0.873134
Trials 49	0.876923	0.956522	0.91791
Trials 50	0.885246	1	0.947761
Trials 51	0.855072	1	0.925373
Trials 52	0.815385	1	0.910448
Trials 53	0.90625	1	0.955224

Continued on next page

Table 1 – *Continued from previous page*

Trials	Specificity	Sensitivity	Accuracy
Trials 54	0.935484	0.902778	0.91791
Trials 55	0.896552	1	0.955224
Trials 56	0.896552	1	0.955224
Trials 57	0.967213	1	0.985075
Trials 58	0.90411	1	0.947761
Trials 59	0.90411	1	0.947761
Trials 60	0.90625	1	0.955224
Trials 61	0.905405	1	0.947761
Trials 62	0.945946	1	0.970149
Trials 63	0.955224	1	0.977612
Trials 64	0.876923	0.956522	0.91791
Trials 65	0.876923	0.956522	0.91791
Trials 66	0.927536	1	0.962687
Trials 67	0.815385	1	0.910448
Trials 68	0.815385	1	0.910448
Trials 69	0.935484	1	0.970149
Trials 70	0.896552	1	0.955224
Trials 71	0.955224	1	0.977612
Trials 72	0.896552	1	0.955224
Trials 73	0.967213	1	0.985075
Trials 74	0.90411	1	0.947761
Trials 75	0.768116	1	0.880597
Trials 76	0.90411	1	0.947761
Trials 77	0.921875	1	0.962687
Trials 78	0.905405	1	0.947761
Trials 79	0.935484	1	0.970149
Trials 80	0.905405	1	0.947761
Trials 81	0.723077	1	0.865672
Trials 82	0.9375	0.971429	0.955224
Trials 83	0.955224	1	0.977612
Trials 84	0.898551	1	0.947761
Trials 85	0.935484	1	0.970149
Trials 86	0.967213	1	0.985075
Trials 87	0.90625	1	0.955224
Trials 88	0.955224	1	0.977612
Trials 89	0.855072	1	0.925373
Trials 90	0.935484	1	0.970149
Trials 91	0.967213	1	0.985075
Trials 92	0.90625	1	0.955224
Trials 93	0.955224	1	0.977612
Trials 94	0.811594	1	0.902985
Trials 95	0.935484	1	0.970149
Trials 96	0.967213	1	0.985075
Trials 97	0.90625	1	0.955224
Trials 98	0.955224	1	0.977612
Trials 99	0.884058	1	0.940299
Trials 100	0.935484	1	0.970149
Trials 101	0.967213	1	0.985075
Trials 102	0.921875	1	0.962687
Trials 103	0.955224	1	0.977612
Trials 104	0.855072	1	0.925373
Trials 105	0.935484	1	0.970149
Trials 106	0.967213	1	0.985075
Trials 107	0.90625	1	0.955224
Trials 108	0.955224	1	0.977612
Trials 109	0.768116	1	0.880597

Continued on next page

Table 1 – *Continued from previous page*

Trials	Specificity	Sensitivity	Accuracy
Trials 110	0.935484	1	0.970149
Trials 111	0.967213	1	0.985075
Trials 112	0.90625	1	0.955224
Trials 113	0.790323	1	0.902985
Trials 114	0.806452	1	0.910448
Trials 115	0.847458	1	0.932836
Trials 116	0.955224	1	0.977612
Trials 117	0.847458	1	0.932836
Trials 118	0.917808	1	0.955224
Trials 119	0.885246	1	0.947761
Trials 120	0.915493	1	0.955224
Trials 120	0.915493	1	0.955224
Trials 121	0.768116	1	0.880597
Trials 122	0.915493	1	0.955224
Trials 123	0.944444	1	0.970149
Trials 124	0.90625	1	0.955224
Trials 125	0.891892	1	0.940299
Trials 126	0.851351	1	0.91791
Trials 127	0.955224	1	0.977612
Trials 128	0.955224	1	0.977612
Trials 129	0.876923	0.869565	0.873134
Trials 130	0.876923	0.956522	0.91791
Trials 131	0.885246	1	0.947761
Trials 132	0.855072	1	0.925373
Trials 133	0.815385	1	0.910448
Trials 134	0.90625	1	0.955224
Trials 135	0.935484	0.902778	0.91791
Trials 136	0.896552	1	0.955224
Trials 137	0.896552	1	0.955224
Trials 138	0.967213	1	0.985075
Trials 139	0.90411	1	0.947761
Trials 140	0.90411	1	0.947761
Trials 141	0.90625	1	0.955224
Trials 142	0.905405	1	0.947761
Trials 143	0.945946	1	0.970149
Trials 144	0.955224	1	0.977612
Trials 145	0.876923	0.956522	0.91791
Trials 146	0.876923	0.956522	0.91791
Trials 147	0.927536	1	0.962687
Trials 148	0.815385	1	0.910448
Trials 149	0.815385	1	0.910448
Trials 150	0.935484	1	0.970149

7.2 VQGAN

Table 2: The table shows the loss of 150 trials of training the VQGAN model on the ECG and PCG datasets. The metrics displayed are the results of the testing set.

Trials	Loss (MSELoss)
Trials	Loss (MSELoss)
Trial 1	1.105269914
Trial 2	1.389261566

Continued on next page

Table 2 – *Continued from previous page*

Trials	Loss (MSELoss)
Trial 3	1.708691012
Trial 4	1.193374934
Trial 5	1.137712664
Trial 6	1.171916363
Trial 7	1.178850136
Trial 8	1.003692477
Trial 9	1.919066291
Trial 10	1.344409995
Trial 11	1.058164494
Trial 12	1.169801207
Trial 13	1.044235211
Trial 14	1.151821913
Trial 15	0.921550395
Trial 16	1.314847813
Trial 17	1.335058524
Trial 18	1.132752772
Trial 19	1.489972486
Trial 20	1.247963322
Trial 21	1.519247625
Trial 22	1.151825562
Trial 23	1.606890953
Trial 24	1.063866685
Trial 25	1.615517031
Trial 26	1.465440657
Trial 27	1.293799209
Trial 28	1.325007693
Trial 29	0.946179461
Trial 30	0.931897085
Trial 31	1.45791853
Trial 32	1.270278955
Trial 33	1.338485762
Trial 34	1.245341674
Trial 35	1.242795733
Trial 36	2.24459157
Trial 37	1.472949293
Trial 38	1.442298039
Trial 39	1.372303231
Trial 40	1.152978439
Trial 41	1.942520739
Trial 42	1.451520846
Trial 43	1.071759974
Trial 44	1.346848873
Trial 45	1.039863243
Trial 46	1.546707468
Trial 47	1.362138208
Trial 48	1.368649456
Trial 49	1.148035832
Trial 50	1.002246842
Trial 51	1.524708315
Trial 52	1.764537177
Trial 53	1.452899493
Trial 54	1.514785657
Trial 55	1.189736296
Trial 56	1.263878663
Trial 57	1.220757187
Trial 58	1.379265235

Continued on next page

Table 2 – *Continued from previous page*

Trials	Loss (MSELoss)
Trial 59	1.090591667
Trial 60	1.332020726
Trial 61	0.994524177
Trial 62	1.02147617
Trial 63	1.354896834
Trial 64	1.949999931
Trial 65	1.379784838
Trial 66	1.249329799
Trial 67	1.010041563
Trial 68	1.281332234
Trial 69	1.255344488
Trial 70	1.287823682
Trial 71	1.387198209
Trial 72	1.064471415
Trial 73	1.653689924
Trial 74	1.112499514
Trial 75	1.414203216
Trial 76	1.003975639
Trial 77	1.139500462
Trial 78	0.938882377
Trial 79	1.35659906
Trial 80	1.663015637
Trial 81	1.515824034
Trial 82	1.157226324
Trial 83	1.330806061
Trial 84	1.239990053
Trial 85	1.583845269
Trial 86	1.405214053
Trial 87	1.08284393
Trial 88	1.233195145
Trial 89	1.355574495
Trial 90	1.451970419
Trial 91	1.24509412
Trial 92	1.659413039
Trial 93	1.494465326
Trial 94	1.317975695
Trial 95	1.304759151
Trial 96	1.538795391
Trial 97	1.391483807
Trial 98	1.09587586
Trial 99	1.445390607
Trial 100	1.502772246
Trial 101	1.446697444
Trial 102	0.917814882
Trial 103	1.390946089
Trial 104	1.209901291
Trial 105	1.015597698
Trial 106	1.241931823
Trial 107	1.591411326
Trial 108	1.428177019
Trial 109	1.351382289
Trial 110	1.466362136
Trial 111	1.748201041
Trial 112	1.558760836
Trial 113	1.664265349
Trial 114	1.101444048

Continued on next page

Table 2 – *Continued from previous page*

Trials	Loss (MSELoss)
Trial 115	1.40044511
Trial 116	1.791699487
Trial 117	1.873512299
Trial 118	1.383976661
Trial 119	1.186629731
Trial 120	1.575379985
Trial 121	1.434846417
Trial 122	0.946789594
Trial 123	1.156761555
Trial 124	1.402753109
Trial 125	1.625465961
Trial 126	1.898537992
Trial 127	1.294733385
Trial 128	0.987046462
Trial 129	1.58165392
Trial 130	1.571759917
Trial 131	1.060433049
Trial 132	1.534537856
Trial 133	0.954090447
Trial 134	2.063099414
Trial 135	1.317213911
Trial 136	1.423943522
Trial 137	0.928776155
Trial 138	1.059863679
Trial 139	1.396253063
Trial 140	1.46973982
Trial 141	1.239788035
Trial 142	1.158693654
Trial 143	0.942449147
Trial 144	1.629033999
Trial 145	1.585119133
Trial 146	1.209561633
Trial 147	0.957834421
Trial 148	1.960000762
Trial 149	1.340325034
Trial 150	1.288578486

8 References

- [1] David Bau, Jun-Yan Zhu, Hendrik Strobelt, Bolei Zhou, Joshua B. Tenenbaum, William T. Freeman, and Antonio Torralba. GAN Dissection: Visualizing and Understanding Generative Adversarial Networks. *arXiv:1811.10597 [cs]*, December 2018. arXiv: 1811.10597.
- [2] Prakash D, Uma Mageshwari T, Prabakaran K, and Suguna A. *Detection of Heart Diseases by Mathematical Artificial Intelligence Algorithm Using Phonocardiogram Signals*.
- [3] PhysioNet/CinC Challenge 2016: Training Sets.
- [4] Nabina N Rawther and Jini Cherian. Detection and Classification of Cardiac Arrhythmias based on ECG and PCG using Temporal and Wavelet features. 4(4):6, 2015.
- [5] Shahid Ismail, Imran Siddiqi, and Usman Akram. Localization and classification of heart beats in phonocardiography signals —a comprehensive review. *EURASIP Journal on Advances in Signal Processing*, 2018(1):26, December 2018.
- [6] Omer Deperlioglu, Utku Kose, Deepak Gupta, Ashish Khanna, and Arun Kumar Sangaiah. Diagnosis of heart diseases by a secure Internet of Health Things system based on Autoencoder Deep Neural Network. *Computer Communications*, 162:31–50, October 2020.

- [7] Dinesh Surukutla, Karan Bhanushali, and Trupti Patil. Cardiac Arrhythmia Detection Using CNN. *SSRN Electronic Journal*, 2020.
- [8] Abdulhamit Subasi. Biomedical Signals. In *Practical Guide for Biomedical Signals Analysis Using Machine Learning Techniques*, pages 27–87. Elsevier, 2019.
- [9] Bolei Zhou, Aditya Khosla, Agata Lapedriza, Aude Oliva, and Antonio Torralba. Learning Deep Features for Discriminative Localization. In *2016 IEEE Conference on Computer Vision and Pattern Recognition (CVPR)*, pages 2921–2929, Las Vegas, NV, USA, June 2016. IEEE.
- [10] Palani Thanaraj Krishnan, Parvathavarthini Balasubramanian, and Snekhala Umamaheswari. Automated heart sound classification system from unsegmented phonocardiogram (PCG) using deep neural network. *Physical and Engineering Sciences in Medicine*, 43(2):505–515, June 2020.
- [11] Abhishek Das, Harsh Agrawal, C. Lawrence Zitnick, Devi Parikh, and Dhruv Batra. Human Attention in Visual Question Answering: Do Humans and Deep Networks Look at the Same Regions? *arXiv:1606.03556 [cs]*, June 2016. arXiv: 1606.03556.
- [12] Pranav Rajpurkar, Awni Y. Hannun, Masoumeh Haghpanahi, Codie Bourn, and Andrew Y. Ng. Cardiologist-Level Arrhythmia Detection with Convolutional Neural Networks. *arXiv:1707.01836 [cs]*, July 2017. arXiv: 1707.01836.
- [13] Tharindu Fernando, Houman Ghaemmaghami, Simon Denman, Sridha Sridharan, Nayyar Hussain, and Clinton Fookes. Heart Sound Segmentation using Bidirectional LSTMs with Attention. *IEEE Journal of Biomedical and Health Informatics*, 24(6):1601–1609, June 2020. arXiv: 2004.03712.
- [14] A. Almasi, M. B. Shamsollahi, and L. Senhadji. A dynamical model for generating synthetic Phonocardiogram signals. In *2011 Annual International Conference of the IEEE Engineering in Medicine and Biology Society*, pages 5686–5689, Boston, MA, August 2011. IEEE.
- [15] V. Kalaivani. DIAGNOSIS OF ARRHYTHMIA DISEASES USING HEART SOUNDS AND ECG SIGNALS. *Russian Journal of Cardiology*, (1-ENG):35–41, January 2014.
- [16] Chris Olah, Alexander Mordvintsev, and Ludwig Schubert. Feature Visualization. *Distill*, 2(11):10.23915/distill.00007, November 2017.
- [17] M Finlay. The "mobile-phonocardiogram", a new tool in the arrhythmia clinic. *Heart*, 92(7):898–898, May 2006.
- [18] Varsha Garg, Arpit Mathur, Nishant Mangla, and Aman Singh Rawat. Heart Rhythm Abnormality Detection from PCG Signal. In *2019 Twelfth International Conference on Contemporary Computing (IC3)*, pages 1–5, Noida, India, August 2019. IEEE.
- [19] L. Jordaens. A clinical approach to arrhythmias revisited in 2018: From ECG over noninvasive and invasive electrophysiology to advanced imaging. *Netherlands Heart Journal*, 26(4):182–189, April 2018.
- [20] Serkan Kiranyaz, Morteza Zabihi, Ali Bahrami Rad, Turker Ince, Ridha Hamila, and Moncef Gabbouj. Real-time phonocardiogram anomaly detection by adaptive 1D Convolutional Neural Networks. *Neurocomputing*, 411:291–301, October 2020.
- [21] P. Lubail and K.V. Ahammed Muneer. The Heart Defect Analysis Based on PCG Signals Using Pattern Recognition Techniques. *Procedia Technology*, 24:1024–1031, 2016.
- [22] Lars-Jochen Thoms, Giuseppe Collichia, and Raimund Girwidz. Real-life physics: phonocardiography, electrocardiography, and audiometry with a smartphone. *Journal of Physics: Conference Series*, 1223:012007, May 2019.
- [23] Preecha Yupapin, Wardkein, Preecha Yupapin, Phanphaisarn, Koseeyaporn, Roeksabutr, Roeksabutr, Wardkein, and Koseeyapon. Heart detection and diagnosis based on ECG and EPCG relationships. *Medical Devices: Evidence and Research*, page 133, August 2011.
- [24] Matthew D. Zeiler and Rob Fergus. Visualizing and Understanding Convolutional Networks. *arXiv:1311.2901 [cs]*, November 2013. arXiv: 1311.2901.
- [25] Aaron van den Oord, Sander Dieleman, Heiga Zen, Karen Simonyan, Oriol Vinyals, Alex Graves, Nal Kalchbrenner, Andrew Senior, and Koray Kavukcuoglu. WaveNet: A Generative Model for Raw Audio. *arXiv:1609.03499 [cs]*, September 2016. arXiv: 1609.03499.
- [26] Daniel Smilkov, Nikhil Thorat, Been Kim, Fernanda Viégas, and Martin Wattenberg. SmoothGrad: removing noise by adding noise. *arXiv:1706.03825 [cs, stat]*, June 2017. arXiv: 1706.03825.
- [27] Siddique Latif, Muhammad Usman, Rajib Rana, and Junaid Qadir. Phonocardiographic Sensing using Deep Learning for Abnormal Heartbeat Detection. *arXiv:1801.08322 [cs]*, July 2020. arXiv: 1801.08322.

- [28] Stephanie Ger and Diego Klabjan. Autoencoders and Generative Adversarial Networks for Imbalanced Sequence Classification. *arXiv:1901.02514 [cs, stat]*, August 2020. arXiv: 1901.02514.
- [29] Chaoqiang Zhao, Qiyu Sun, Chongzhen Zhang, Yang Tang, and Feng Qian. Monocular Depth Estimation Based On Deep Learning: An Overview. *Science China Technological Sciences*, 63(9):1612–1627, September 2020. arXiv: 2003.06620.
- [30] Amy T. Dao. Wireless laptop-based phonocardiograph and diagnosis. *PeerJ*, 3:e1178, August 2015.
- [31] Sumair Aziz, Muhammad Umar Khan, Majed Alhaisoni, Tallha Akram, and Muhammad Altaf. Phonocardiogram Signal Processing for Automatic Diagnosis of Congenital Heart Disorders through Fusion of Temporal and Cepstral Features. *Sensors*, 20(13):3790, July 2020.
- [32] Md. Khayrul Bashar, Samarendra Dandapat, and Itsuo Kumazawa. Heart Abnormality Classification Using Phonocardiogram (PCG) Signals. In *2018 IEEE-EMBS Conference on Biomedical Engineering and Sciences (IECBES)*, pages 336–340, Sarawak, Malaysia, December 2018. IEEE.
- [33] Cristhian Potes, Saman Parvaneh, Asif Rahman, and Bryan Conroy. Ensemble of Feature-based and Deep learning-based Classifiers for Detection of Abnormal Heart Sounds. September 2016.
- [34] S1 and S2 Heart Sound Recognition Using Deep Neural Networks. *IEEE Transactions on Biomedical Engineering*, 64(2):372–380, February 2017.
- [35] Grzegorz Redlarski, Dawid Gradolewski, and Aleksander Palkowski. A System for Heart Sounds Classification. *PLoS ONE*, 9(11):e112673, November 2014.
- [36] Chengyu Liu, David Springer, Qiao Li, Benjamin Moody, Ricardo Abad Juan, Francisco J Chorro, Francisco Castells, José Millet Roig, Ikaro Silva, Alistair E W Johnson, Zeeshan Syed, Samuel E Schmidt, Chrysa D Papadaniil, Leontios Hadjileontiadis, Hosein Naseri, Ali Moukadem, Alain Dieterlen, Christian Brandt, Hong Tang, Maryam Samieinasab, Mohammad Reza Samieinasab, Reza Sameni, Roger G Mark, and Gari D Clifford. An open access database for the evaluation of heart sound algorithms. *Physiological Measurement*, 37(12):2181–2213, December 2016.
- [37] Ye Jia, Ron J. Weiss, Fadi Biadsy, Wolfgang Macherey, Melvin Johnson, Zhifeng Chen, and Yonghui Wu. Direct speech-to-speech translation with a sequence-to-sequence model. *arXiv:1904.06037 [cs, eess]*, June 2019. arXiv: 1904.06037.
- [38] Mohammed Nabih Ali, EL-Sayed A. El-Dahshan, and Ashraf H. Yahia. Denoising of Heart Sound Signals Using Discrete Wavelet Transform. *Circuits, Systems, and Signal Processing*, 36(11):4482–4497, November 2017.
- [39] K. Ajay Babu, Barathram Ramkumar, and M. Sabarimalai Manikandan. S1 and S2 heart sound segmentation using variational mode decomposition. In *TENCON 2017 - 2017 IEEE Region 10 Conference*, pages 1629–1634, Penang, November 2017. IEEE.
- [40] Wenjie Zhang, Jiqing Han, and Shiwen Deng. Heart sound classification based on scaled spectrogram and partial least squares regression. *Biomedical Signal Processing and Control*, 32:20–28, February 2017.
- [41] M. Abo-Zahhad, Mohammed Farrag, Sherif N. Abbas, and Sabah M. Ahmed. A comparative approach between cepstral features for human authentication using heart sounds. *Signal, Image and Video Processing*, 10(5):843–851, July 2016.
- [42] Elmar Messner, Matthias Zohrer, and Franz Pernkopf. Heart Sound Segmentation—An Event Detection Approach Using Deep Recurrent Neural Networks. *IEEE Transactions on Biomedical Engineering*, 65(9):1964–1974, September 2018.
- [43] Patrick Esser, Robin Rombach, and Björn Ommer. Taming Transformers for High-Resolution Image Synthesis. *arXiv:2012.09841 [cs]*, February 2021. arXiv: 2012.09841.
- [44] Photo Posters - Create Custom Photo Posters | Walgreens Photo.
- [45] Ye Jia, Ron J. Weiss, Fadi Biadsy, Wolfgang Macherey, Melvin Johnson, Zhifeng Chen, and Yonghui Wu. Direct speech-to-speech translation with a sequence-to-sequence model. *arXiv:1904.06037 [cs, eess]*, June 2019. arXiv: 1904.06037.